

Small Antennas for Mobile and Ultra-Wideband Communication

D. Heberling, D. Manteuffel, M. Martínez-Vázquez, M. Geissler, O. Litschke

IMST GmbH

Carl-Friedrich-Gauß-Straße 2, D-47475 Kamp-Lintfort, Germany

heberling@imst.de

Abstract

Mobile communication is an enormous growing market of communication and has a strong influence on the RF and microwave world. While UMTS is on the way of installation and going into business, new communication system technologies can be seen at the horizon of the communication world. One of this is UWB, the ultra wideband communication. This promising technology can become the important broadband communication technology for wireless multimedia systems. It is based on a concept that can be seen as impulse radio communication and uses a bandwidth of at minimum 500MHz and more. Beside of communication this technology allows due to the impulse concept a localisation of the mobile unit. It functions similar to a radar concept. At the moment UWB is on the way towards standardisation in Europe and a lot of effort is invested to develop the hardware necessary for realisation.

This tutorial shows in a first part the state of the art in today's antenna technology for mobiles. This includes not only handsets but also new systems that are expected to come up with the UMTS and WLAN. The second part will consider the ultra wide band technology. This fairly new technology asks for many new approaches not only in the field of system design and propagation but also for the hardware and antennas.

1. Small Antennas for Mobiles

Integrated antennas have become very popular due to the advantages they provide with respect to the aesthetical design of mobile phones. Yet, a drawback is that the limited space for the antenna module within the casing of the cell phone generally results into narrow bandwidth antenna solutions. This problem becomes even more serious when a multiband antenna has to be designed. On the other side it is obvious that there is a strong interaction between the antenna-module and the board of the mobile phone on one hand and the antenna with user on the other hand. Only a careful design of the antenna taking this interaction into account can result in antennas that fulfil today's requirements for handsets.

The advent of new mobile communications devices is a real challenge for antenna designers, as they have to implement integrated multiband operation within very different kinds of terminals like PCMCIA-card modules, using sometimes more than one input port. It's getting more and more important to characterise very careful the efficiency of such radiation systems. The Wheeler-Cap Method is a promising way to do this.

1.1 Dual Band Antenna Concepts

A typical approach to realise a dualband antenna is based on two resonating elements within one antenna module (Figure 1). The problem arising is that the coupling of the combined elements has an additional effect on the resonance's especially in the upper frequency range. With some modifications it is possible to succeed in a proper matching for a single feed solution in both frequency bands.

Another possibility to enlarge the bandwidth of an antenna is the use of parasitic elements. This principle is widely reported in the literature [1] for microstrip patch antennas. An application for mobile phone antennas has recently been published in [2]. Figure 2 shows the two radiator dualband antenna in combination with a parasitic element. The parasitic element is situated above the original antenna at the top of the phone. As the height of the parasitic element is lower than the original antenna-module this additional space (0.4 cm^3) is available at this position taking into account a curved casing at the top of the phone. In Figure 2 the resonators for the upper frequencies are placed

orthogonal to each other. This provides less coupling from the electric nearfield of the resonators compared to having the parasitic resonator in parallel to the DCS resonator. Nevertheless the other configuration works also, as it is reported in [2]. By using a parasitic element the bandwidth can be increased by a large amount. Therefore it is interesting especially for future applications where more frequency bands have to be covered by only one antenna. On the other hand with a parasitic element matching becomes more complicated because more parameters compared to the original antenna have to be considered.

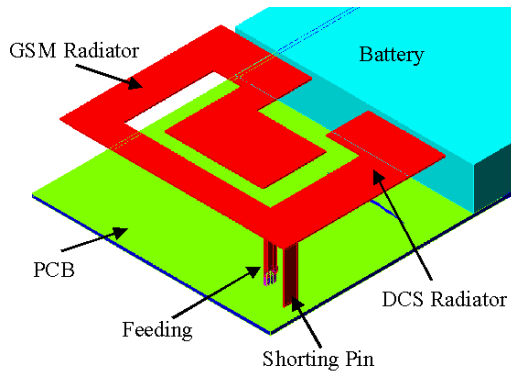
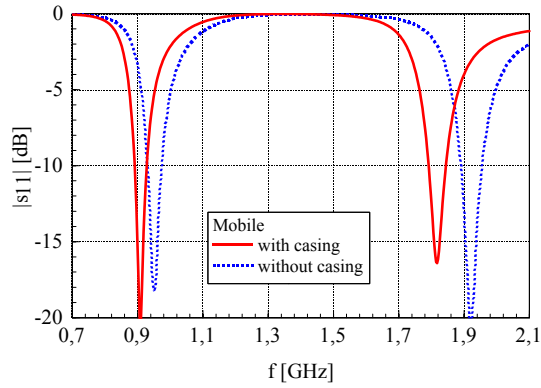


Figure 1: a) Dualband antenna



b) Matching with/without casing

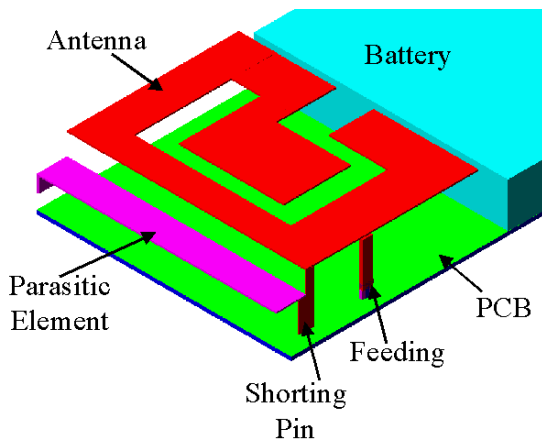
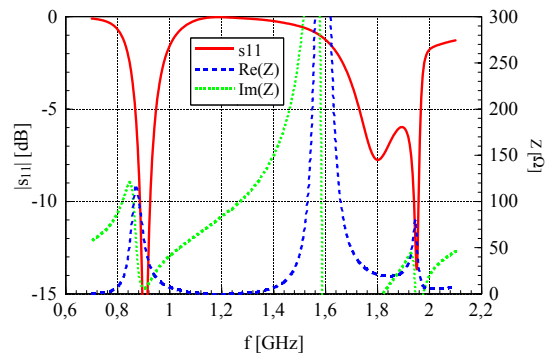


Figure 2: a) Integrated antenna with parasitic element



b) Matching and impedance behaviour

1.2 Space Efficient Tripleband Antenna Concept

In order to achieve large bandwidth for the upper frequency range, the concept of parasitic resonances, known from the theory of microstrip antennas, is applied. Using a slot to generate a parasitic resonator, like originally proposed in [3] for a standard microstrip antenna, requires only minor increase in size of the antenna module compared to an additional metal strip as proposed in [2]. Figure 3a shows a sketch of the general configuration. The antenna consists of an outer strip (1) that surrounds an inner strip (2), a slot (3) is cut into the outer strip (1). Figure 3b shows a prototype of an antenna module based on this concept.

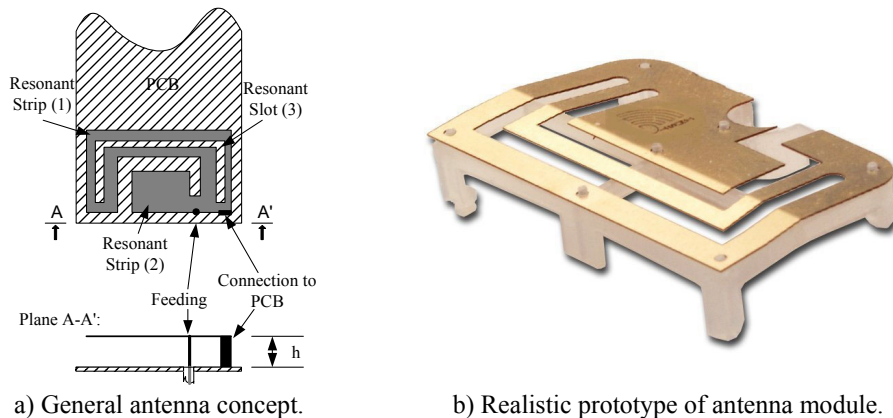


Figure 3: Prototype of a triple band antenna and the exemplary electrically nearfield

1.3 Interaction of small antennas with the environment

Taking a closer look on a canonical model of a mobile phone the generalized current distribution can be divided into three portions (see Figure 4):

As a first portion we can identify the current distribution on the antenna module itself. For a $\lambda/4$ antenna with shorting pin at one end of the patch, the current distribution follows a $\lambda/4$ distribution all along the patch modified only by some edge effects on the patch and capacitive coupling of different parts of the patch due to folding the track. If this $\lambda/4$ antenna module is positioned on the PCB (Printed Circuit Board) of the mobile, a current distribution similar to the one on the antenna module, but opposite in phase is induced on the antenna side of PCB right under the antenna module. The field generated by this second portion of the current distribution interferes with

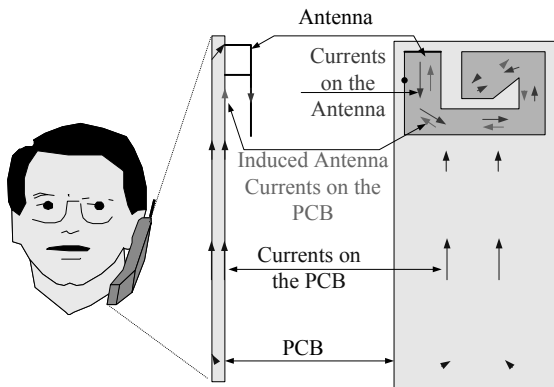


Figure 4: Generalized current density distribution on a mobile phone.

the field generated by the current distribution on the antenna module and is mainly cancelled in some distance from the mobile. The third portion is excited on the PCB, too. As the PCB of modern mobile phones is not large compared to the wavelength, it cannot be considered as a simple ground plane for the $\lambda/4$ antenna module. Due to the specific dimensions of the PCB, the antenna module excites a current distribution on the PCB which is related to the boundary conditions of this conductive plate. For frequencies within the GSM900 band this may be around the $\lambda/2$ resonance of the PCB; for frequencies within the GSM1800 band this may be around the λ resonance respectively. In [2] this phenomenon has been investigated in more detail deriving an equivalent circuit of the mobile which contains one resonator representing the antenna module and another resonator representing the PCB.

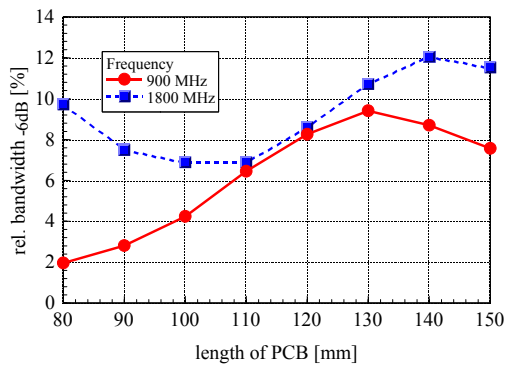


Figure 5: Interaction of antenna-module and PCB: Influence on the bandwidth.

1.4 Interaction of the antenna with the board

Due to the ongoing miniaturization of components and for marketing requirements the size of modern mobile phones decreases. Typical lengths vary between 80 mm and 130 mm. Assuming a quarter-wave antenna on a small PCB, it is obvious that there is a strong interaction between the antenna-module and the board [4]. Figure 5 gives the behaviour of the bandwidth of integrated antennas on a PCB of different length. It can be observed from Figure 5 that the resonance effect of the board can have a large impact on the impedance bandwidth of the resulting antenna system [5], [6]. Especially for 900 MHz the bandwidth becomes very low for a small mobile.

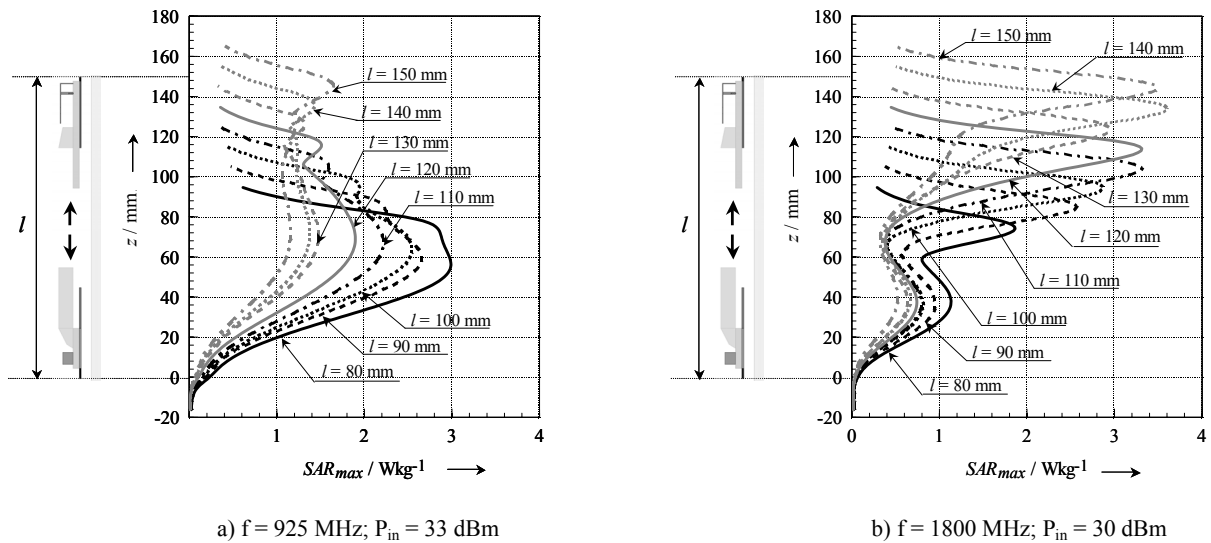


Figure 6: SAR_{max} on the surface of a flat phantom for different models of a mobile equipped with an integrated C-Patch antenna

1.5 Interaction of the antenna with the user

The other important interaction that needs to be taken into account is the coupling of the antenna with the user. Not only the upcoming request of the users of mobile phones to know about the electromagnetic field impact in the user's body asks for a careful analysis of the coupling, but for an accurate design it is also necessary to take into account the influence of the lossy body beside the small antenna. In terms of SAR it is interesting to see how the resulting current distribution couple to the tissue of the users head. In order to see the pure correlation of the current distribution on the mobile with the SAR in the tissue, the numerical model of the mobile is placed in front of a flat phantom to avoid any influences due to the anatomical shape of a real head.

As published in [7] Figure 6a shows the maximum SAR along the axis of the mobile on the surface of the flat phantom for eight different models of a mobile phone equipped with an integrated C-Patch antenna operating at 925 MHz. The input power at the antenna feeding point is scaled to $P_{in} = 33$ dBm. The simulation model of the mobile phone does not account for any losses. The distance between the PCB and the flat phantom is 5 mm. It can be observed that the SAR distribution on the surface of the flat phantoms contains two local maxima for each model investigated. With respect to the generalized current distribution described above, it can be noticed that the maximum relative to the mid height of the mobile is related to the current distribution on the PCB. The other maximum relative to the top of the phone is related to the current distribution near the antenna feeding point. For all mobile phones smaller than 130 mm the maximum due to the current distribution on the PCB contains the highest SAR value. Additionally, using this length of the PCB ($l = 130$ mm) both maxima are nearly equal and the total maximum SAR is smaller compared to all other models.

Figure 6b shows the same kind of investigation for an antenna module operating at $f = 1800$ MHz. The input power at the antenna feeding point is scaled to $P_{in} = 30$ dBm. Similar to the investigation for the GSM900 frequency range two local maxima can be observed for the SAR distribution of each mobile. The maximum due to the current distribution at the antenna feeding point contains the highest SAR value in any case investigated at this frequency.

1.6 Antenna for PCMCIA Application

The increasing demand for access to mobile communications through portable equipment such as notebooks or PDAs with the use of PCMCIA cards requires the development of integrated, multiband antennas as shown in Figure 7. This helps to provide the desired connectivity, through the access to cellular or private networks. Therefore, both mobile cellular standards, such as the GSM family, and third generation standards such as UMTS, as well as unlicensed network accesses, like WLAN, should be implemented into a single device. Up to now, wire antennas such as monopoles or helix have been widely implemented into such antenna systems. But as users request more compact equipment, the trend leads to integrated solutions, like patch antennas, which should provide high efficiency and optimal performance, while keeping a reduced size. Again, as multiple standards have to be covered, multiresonant metallic patches are frequently used. These are both cost-effective and straightforward to produce and mount, whereas their inherent flexibility allows adapting them to the available antenna volume.

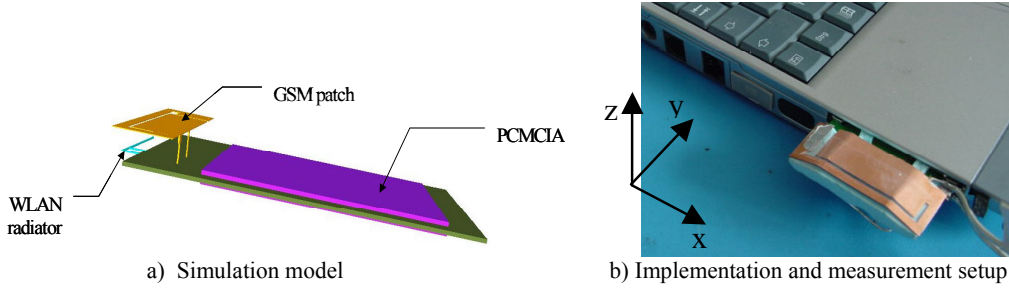


Figure 7: Multiband PCMCIA antenna

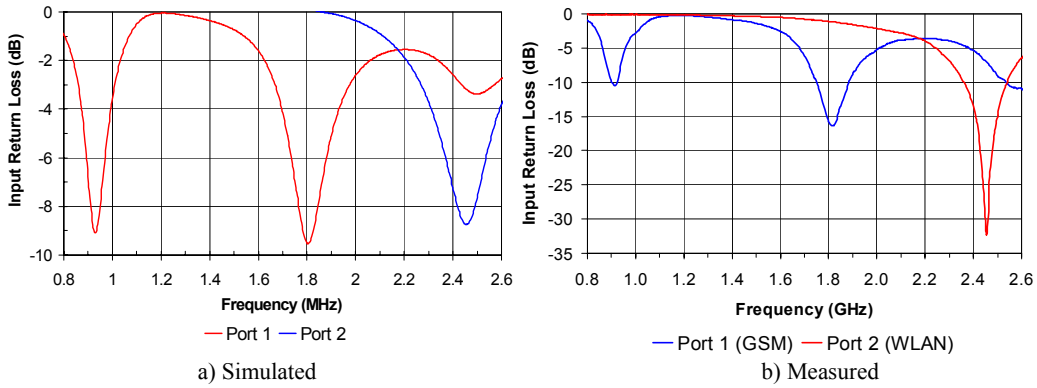


Figure 8: input return loss. Port 1: GSM 900/1800/1900, Port 2: WLAN

The structure of the antenna for PCMCIA is presented in Figure 7a. Figure 7b displays the current implementation of the structure, with two cables added for measurement purposes. A PIFA [8] concept was chosen to cover the GSM bands. It consists of a probe-fed metal plate with a shorting pin, which allows obtaining two separate resonances: the first one for the GSM 900 band, the second one for both GSM 1800 and GSM 1900. Indeed, though multiple resonances are usually used to cover these two overlapping bands, a single mode providing enough bandwidth can also be used. Also, an Inverted-F antenna (IFA) was added, to ensure the access to WLAN. It consists of a shorted wire printed onto a non-metallised area of the PCB board. The GSM 900/1800/1900 antenna occupies a volume of 50mm x 18mm x 8mm, whereas a surface of 29mm x 6mm was reserved for the WLAN IFA. The overall size of the PCMCIA board is 54mm x 110mm. Figure 8 gives the simulated and measured matching characteristic of the antenna.

1.7 Efficiency of small antennas

Efficiency represents an important parameter when determining the radiation performance of a mobile handset, as it gives the ratio between the power delivered to the antenna and the power that is actually radiated.

Wheeler introduced a method for determining the radiation efficiency of antennas by performing two measurements, the first one in free space and the second one within a closed sphere [9]. He assumes, that the antenna at resonance frequency can be modelled as two series resistances; the radiation resistance R_{rad} and the loss resistance R_L . The first measurement delivers the sum of both contributions R_1 , the second measurement delivers R_2 , which corresponds to R_L . The radiation efficiency can be calculated as [10]

$$\eta_{rad} = \frac{R_{rad}}{R_L + R_{rad}} = \frac{R_1 - R_2}{R_1}$$

Several investigations show, that one can obtain good results for electrically small antennas. However, all these investigations focus on antennas directly mounted on the ground plane, e.g. loop antennas or patch antennas [10], [11]. Antennas of small mobile devices however do not use large ground planes. They are typically mounted on the top side or the back side of the mobile device, and the device acts as an active counter pole of the antenna. Therefore, the whole device has to be considered in order to determine the radiation efficiency correctly.

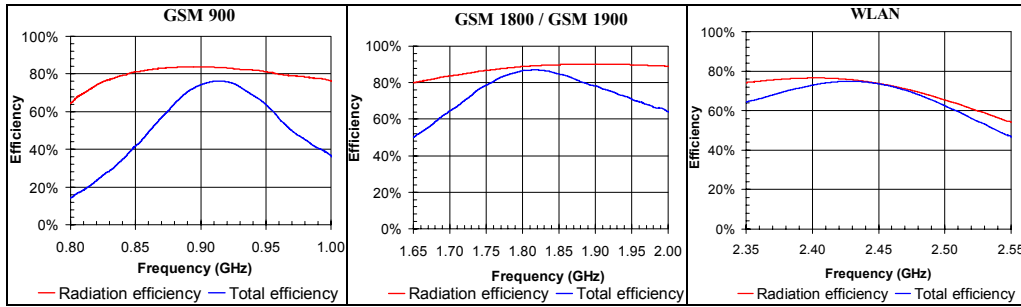


Figure 9: Measured antenna efficiency of the PCMCIA antenna

In [12] an improved model is defined, describing the cap as a small ohmic resistance R_{cap} connected via a transmission line. Its length l_{cap} describes the effective electrical distance between the device and the cap. R_{cap} is typically negligible when compared to the measured resistances. Using this new equivalent circuit, the extraction of the efficiency is more complex. Johnston [13] describes a method to calculate the transmitted power by measuring the same antenna within several box dimensions, using a sliding wall. These measurements cause a circle in the Smith chart and the transmitted power can be directly determined [12].

This improved Wheeler-cap method was used to characterise the radiation efficiency of the above described PCMCIA antenna. The obtained results are displayed in Figure 9.

A distinction was made between radiation efficiency, determined by the patch itself, and the total efficiency, which includes the effect of matching losses. If the matching were perfect, both curves would be superposed. As radiation efficiency is higher and more constant over the frequency than the total efficiency, bandwidth restrictions are not caused by the antenna itself but by mismatching.

2. Antennas for Ultra Wide Band Systems

Ultra Wide Band radio technology is one of the future technologies for mobile communication. It uses pulse position modulation of very short duration pulses which results in a PSD which, although very broad (over 1 GHz starting almost from DC), has only a few μW per MHz. This feature makes it resistant to jamming which could be a key requirement for mobile computing. Due to the wide bandwidth (or very short pulses), it is easier to fight multipath effect. Also the signal has a higher penetrating power that makes it suitable for purposes other than simple data communication, like Ground Penetrating Radar, Position locator inside a building etc.

During the last years, a standardisation and regulation of the ultra wide band technologie is on the way. In April 2002, after extensive commentary from industry, the FCC issued its First Report and Order on UWB technology [14], there by providing regulations to support deployment of UWB radio systems. The FCC regulations classify UWB applications into several categories with different emission regulations in each case. Maximum emissions in the prescribed bands are at an effective isotropic radiated power (EIRP) of -41.3 dBm per MHz, and the -10 dB level of the emissions must fall within the prescribed band. In addition, for a radiator to be considered to UWB, the 10 dB bandwidth $f_H - f_L$ must be at least 500 MHz, and the fractional bandwidth, $2(f_H - f_L)/(f_H + f_L)$, must be at least 0.2, as determined by the -10 dB power points f_H and f_L . Figure 10 shows the draft specification masks for Europe and FCC.

2.1 Propagation aspects of UWB

When going from wideband (WB) to ultra-wideband (UWB) radio channel modeling, a number of aspects have to be taken into account that amount to a changed overall behavior of the channel. In particular, the assessment of transmitted and received waveforms requires accurate and coherent models for each part of the channel. For example, a prominent phenomenon found for wideband channels is frequency selectivity which leads to dispersion of the transmitted signal. In many cases frequency selectivity can be attributed mainly to propagation effects (multipath) while dispersion effects introduced by the antennas may be less significant. For impulse radio applications, however, even the dispersive properties of antennas have to be considered carefully. Figure 11 shows a typical average power delay profile (APDP) based on 30×30 baseband impulse responses taken on a $30 \text{ cm} \times 30 \text{ cm}$ grid under LOS conditions in an office

environment. The measurement band is 1-11 GHz, giving a nominal delay resolution of 100 ps (corresponding to 3 cm spatial resolution). Two global observations can be made here: First, the APDP is dominated by the LOS component arriving at about 8 ns, and for delays exceeding app. 30 ns, the APDP exhibits a single diffuse multipath

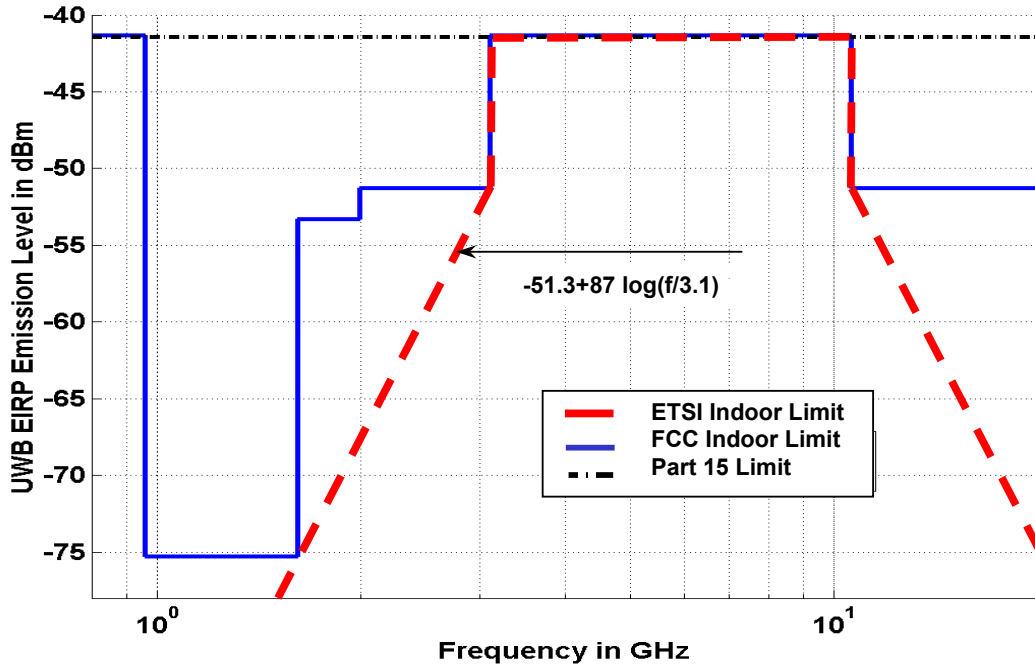


Figure 10: UWB regulation in Europe, draft specification mask

(MP) cluster caused by superposition of a large number of unresolved paths. Second, in the delay range 8-30 ns, the MP cluster envelope deviates from a simple exponential decay behavior, and a number of strong echoes embedded in the surrounding MP components (MPC) can be clearly recognized. The high bandwidth of 10 GHz allows to resolve individual paths that correspond to specific interactions; by comparison with the geometry of the measurement environment, many of the strong echoes can be mapped to individual paths that undergo particular interactions including for example wall reflections, ceiling-wall reflections etc.

Figure 12 shows color-coded power delay profiles for 150 impulse responses. These responses were obtained by displacing the Tx antenna along a straight line of 150 cm length such that the direction of movement was roughly perpendicular to the Rx-Tx direction; the distance between Rx and Tx was approximately 3 m. According to the direction of movement the delay of various MPCs changes.

A very simple, but nevertheless distinguishing feature of UWB is that these resolution capabilities are made available at room scale. It is obvious that a channel model suitable e.g. for positioning applications necessarily has to consider these essential UWB channel features. At some points in the plot, several traces intersect each other. In these regions a regular fading pattern is clearly recognizable that, unlike what is observable in the WB case, nicely illustrates the result of the superposition of just two individual paths.

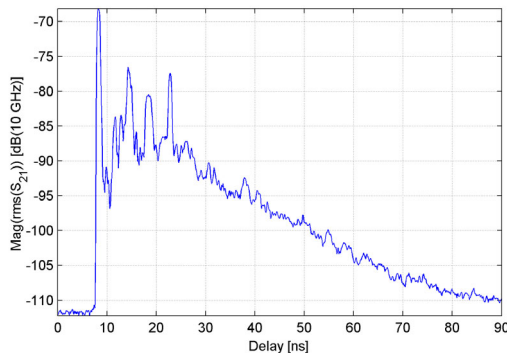


Figure 11: UWB Example for UWB average power delay profile [15]

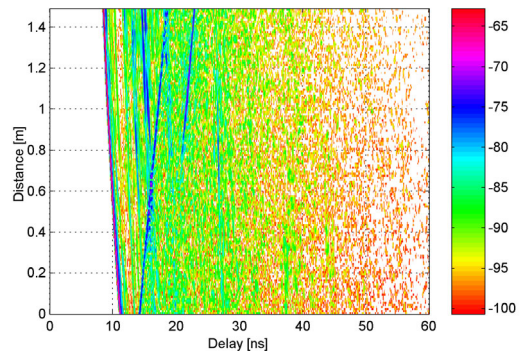


Figure 12: Color-coded power delay profiles for 150 baseband impulse responses along 150 cm of Tx displacement almost perpendicular to the Rx-Tx line of sight.

2.2 Antenna design for UWB systems

Ultra wideband radio systems are characterized by multi-octave to multi-decade frequency bandwidths, and are expected to transmit and receive baseband pulse waveforms with minimum loss and distortion. Both transmit and receive antennas can affect the faithful transmission of UWB signal waveforms because of the effects of impedance mismatch over the operating bandwidth, pulse distortion effects, and the dispersive effects of frequency dependent antenna gains and spreading factors [16]. For example, antennas behave like direction-sensitive filters over ultra-wide bandwidths, and the signal driving the transmitting antenna, the electric far-field (even in free space), and the signal across the receiver load may differ considerably in wave shape and spectral content. Ideally matched correlation receivers are difficult to realize.

Some of the desirable antenna characteristics for UWB radio systems are:

- wide impedance bandwidth
- fixed phase centre over frequency
- high radiation efficiency

Good impedance matching over the operating frequency band is desired to minimize reflection loss, and to avoid pulse distortion. If the phase centre (the point where spherical wave radiation effectively originates) of an antenna moves with frequency (as is the case with spiral, log periodic, and travelling wave antennas), pulse dispersion will occur. The desire for high radiation efficiency is self-evident, but several types of broadband antennas employ resistive loading, which reduces efficiency. Other UWB antenna concerns include polarization properties (versus frequency), physical size, cost, and feeding techniques (balanced vs. unbalanced). For example the electrically short dipole provides good pulse fidelity, but at a relatively low amplitude. The resonant dipole provides a higher amplitude, but also greater duration. The log-periodic dipole array has very good impedance and gain bandwidth, but the non-constant phase centre causes considerable ringing of the radiated field. In contrast, the constant phase centre of the Vivaldi antenna produces less ringing, and a very high amplitude pulse.

2.3 Antenna design for UWB systems

From a signal processing point of view the antenna can be considered a LTI (Linear Time-Invariant) system which can be fully characterized by its transfer function [15]. This can be expressed by

$$\frac{\mathbf{E}_2(\mathbf{r}_2, \omega)}{\sqrt{Z_{F0}}} = \frac{U_{1,in}(\omega)}{\sqrt{Z_L}} \mathbf{A}_{TX}(\hat{\mathbf{r}}_{12}, \omega) \frac{e^{-jk_0 r_{12}}}{\sqrt{4\pi r_{12}}}. \text{ Hereby denotes } \mathbf{E}_2(\mathbf{r}_2, \omega) \text{ the electric field strength at a point } \mathbf{r}_2 \text{ in}$$

the farfield of the antenna at \mathbf{r}_1 which is excited by an incoming voltage $U_{1,in}(\omega)$ at the antenna port (see Figure 13). While $e^{-jk_0 r_{12}}/\sqrt{4\pi r_{12}}$ describes the propagation of the wave from the antenna to the observation point in the direction \mathbf{r}_{12} , $\mathbf{A}_{TX}(\hat{\mathbf{r}}_{12}, \omega)$ represents the transmit transfer function of the antenna. Z_{F0} and Z_L are the free space and feed line impedance, respectively and $\hat{\mathbf{r}}_{12} = \mathbf{r}_{12}/r_{12}$ is the unit vector from the antenna to the observation point. Consequently $\mathbf{A}_{TX}(\hat{\mathbf{r}}_{12}, \omega)$ is independent from the distance between the antenna and the observation point but one has always to take into account that the definition of the transfer function requires local plane wave propagation and thus is related to farfield conditions only.

On the other hand, following [15] the reception of the antenna from an incident plane wave can be expressed by

$$\frac{U_{2,out}(\omega)}{\sqrt{Z_L}} = \sqrt{4\pi} \frac{\mathbf{E}_{1,inc}}{\sqrt{Z_{F,0}}} \mathbf{h}_{RX}(\hat{\mathbf{k}}, \omega). \text{ Hereby denotes } U_{2,out}(\omega) \text{ the voltage traveling out of the antenna into the}$$

receiving system if the antenna is exposed to a plane wave. Note that $\mathbf{E}_{1,inc}$ is the electric field strength of an incident plane wave, i. e., the field in absence of the antenna. With this definition $\mathbf{h}_{RX}(\hat{\mathbf{k}}, \omega)$ can be considered as the receive transfer function of the antenna. Figure 13 illustrates the above definitions.

Both, transmit and receive transfer functions are related to each other by Lorentz theorem of reciprocity. An expression that takes into account the ultra wideband properties of the system has been derived in [15]:

$2j\omega \mathbf{h}_{RX}(-\hat{\mathbf{k}}, \omega) = c_0 \mathbf{A}_{TX}(\hat{\mathbf{k}}, \omega)$ Coming back to the purpose of our investigation this means that it is sufficient to calculate the transmit transfer function on the basis of a FDTD simulation in order to fully characterize the antenna.

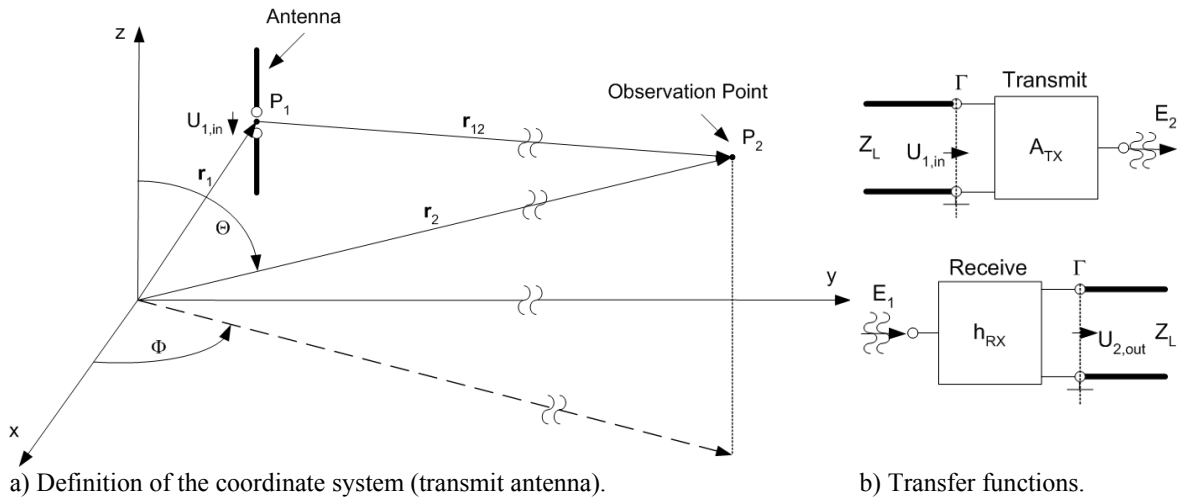


Figure 13: Representation of the antenna as an LTI system for transmit and receive mode.

2.4 Results

In order to prove the above derived method a biconical antenna is analyzed. The antenna is designed to operate in the frequency range above 3.1 GHz. For the FDTD simulation the antenna is modeled with all necessary details. PML (Perfectly Matched Layer) absorbing boundaries are positioned in the nearfield of the antenna. The distance to the PML boundaries is less than $\lambda/4$ at the lowest frequency of interest thus resulting in a time and memory efficient simulation. The antenna is excited by a broadband Gaussian pulse centered at 0 Hz and having a half bandwidth of 20 GHz with reference to a signal decrease of 20 dB. The nearfield of the antenna is recorded at every 200 MHz between 1 GHz and 20 GHz on a Huygens surface enclosing the antenna. The EMPIRETM [17] software package uses this nearfield data to derive equivalent electric and magnetic sources on the surface and extrapolate the field strength in the farfield. The total simulation time, including the post-processing of the farfield data, takes only a few minutes on a standard 2 GHz PC. The results from this simulation are used to process the transmit and receive transfer functions of the antenna according to the above mentioned method. To validate the approach a second simulation model is set up that consists of two biconical antennas separated by distance of $d = 50$ cm. While the first antenna is fed by the Gaussian pulse the second antenna is passive and receives the radiated pulse from the field. Therefore it is possible to calculate the transmission between both antennas in terms of s_{21} .

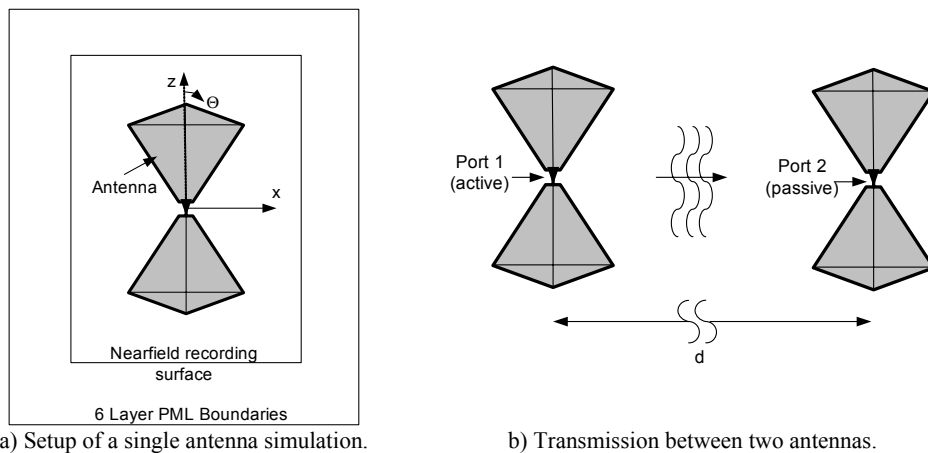


Figure 14: Setup for one-antenna simulation and transmission between two antennas.

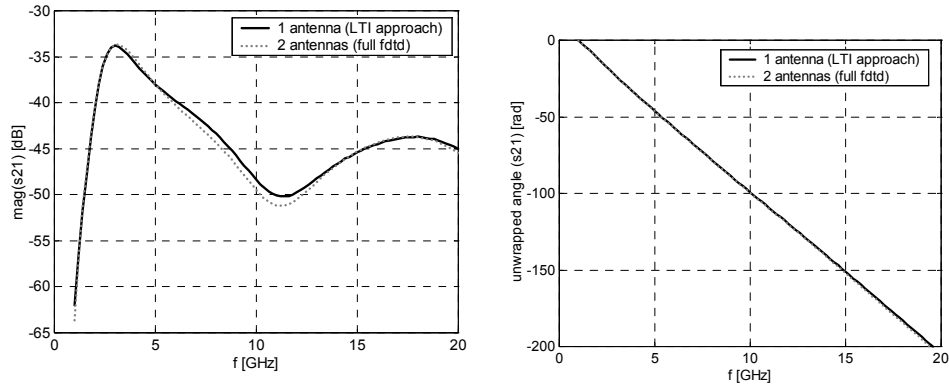


Figure 15: Transmission between two antennas calculated by the complete FDTD simulation of two antennas and the FDTD simulation of a single antenna combined with a LTI approach.

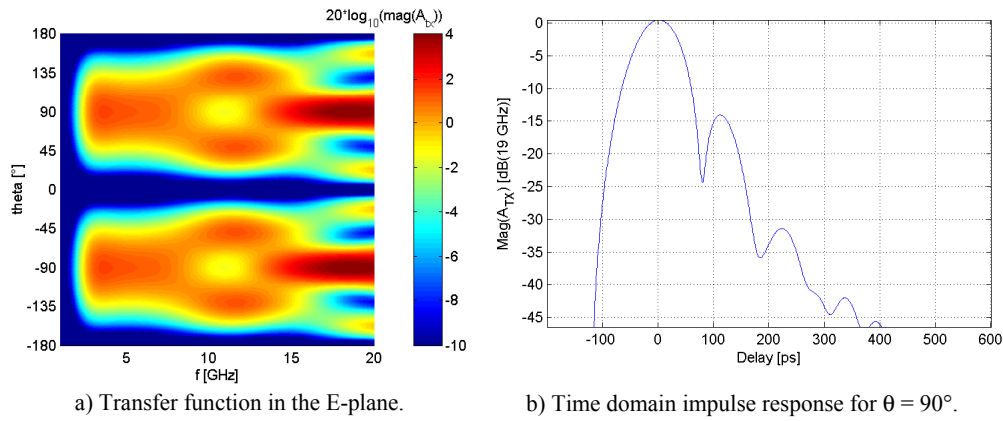


Figure 16: TX characteristics of the biconical antenna.

In addition to the direct calculation of s_{21} based on the complete FDTD simulation of two antennas, we can also use the transfer functions from the one-antenna simulation and calculate the transmission between two antennas by the following expression [15]: $s_{21}(\omega) = \frac{b_2}{a_1} \Big|_{a_2=0} = \mathbf{A}_1(\hat{\mathbf{k}}_{12}, \omega) \mathbf{h}_2(\hat{\mathbf{k}}_{12}, \omega) \frac{e^{-jk_0 d}}{d}$. Figure 15 compares the results from both

methods and shows a good agreement. This proves that the method described above has been implemented in the correct way. In addition to the validation aspect of such a calculation it should be noted that it is now possible to fully characterize an antenna by a simple single nearfield FDTD simulation of the transmitting antenna. Furthermore the TX- and RX-transfer functions can be used e. g. for later propagation simulations using other simulation tools.

Coming back to the characterization of the single antenna Figure 16a illustrates the TX transfer function of the biconical antenna in the E-Plane. It can be observed that the antenna is matched above 3 GHz. The characteristics reminds of a simple 1st order dipole until a frequency of 8 GHz. For higher frequency the characteristic changes showing sidelobes and gain deviations. Figure 16b shows the magnitude of the baseband impulse response of the antenna for $\theta=90^\circ$, giving a clear indication of the *ringing* behavior of the antenna. The impulse response has been determined using a Kaiser-Bessel frequency domain window.

2.5 Application example

The proposed method has been established to characterise UWB antennas in their specific user situation. A typical scenario is a small antenna which is integrated in the chassis of a home entertainment application such as a DVD player.

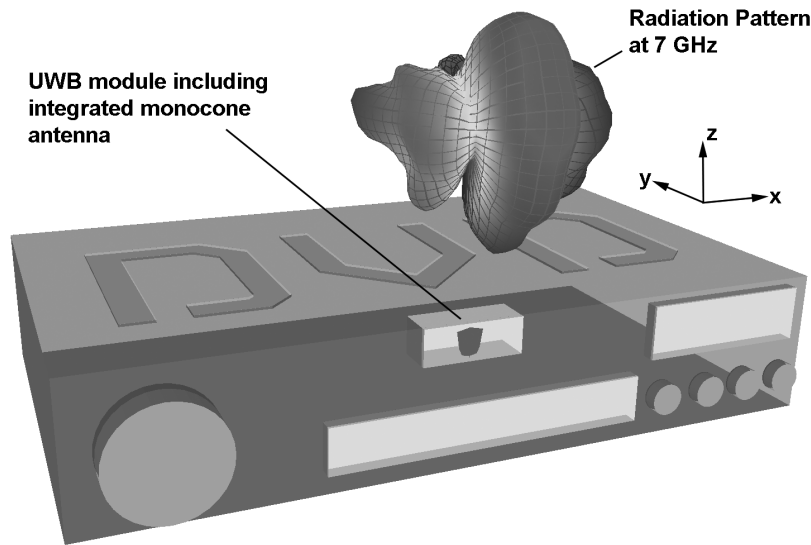


Figure 17: UWB module including an integrated monocone antenna in a DVD player. Calculated Radiation pattern at $f = 7$ GHz.

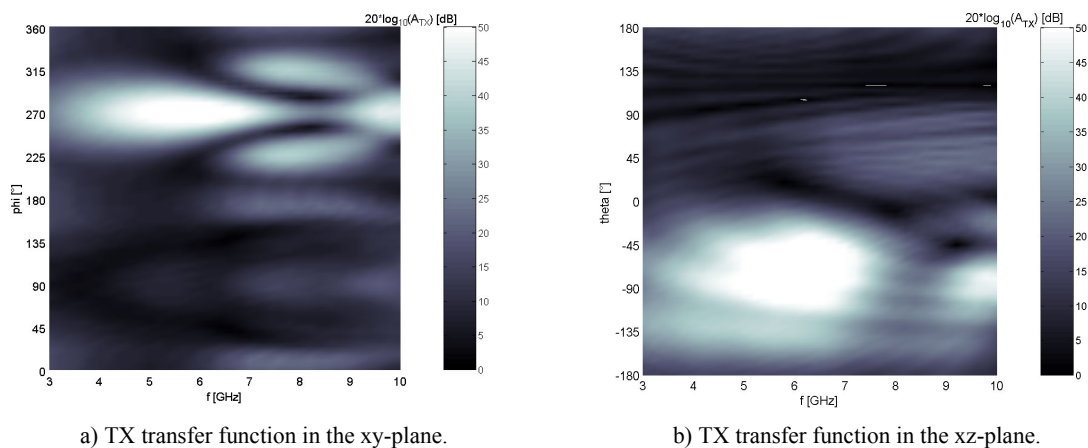


Figure 18: Calculated TX transfer function of the monocone antenna integrated into the UWB module inside a DVD player.

Figure 17 shows the numerical model of a DVD player having an integrated UWB module including a monocone antenna. Although the UWB module provides some air-filled space with only small windows at the top and at the front around the monocone, the entire module can be seen as integrated in a large metal box. Therefore, it is obvious that the specific integration scenario has a significant effect on the radiation pattern of the antenna. For illustration purposes, the 3D radiation pattern at 7 GHz is displayed as well in Figure 17. Having in mind the more or less omnidirectional radiation pattern of a monocone antenna in free space, the pattern of the antenna integrated in DVD player shows strong directivity.

Based on an FDTD simulation including the whole DVD player, the transmit transfer functions of the antenna is calculated. It can be observed in Figure 18 that the radiation pattern of the monocone antenna shows a single main beam up to 6 GHz, and sidelobes occurring at higher frequencies. Furthermore, it is clearly illustrated that there are shadow areas located at the backside of the DVD player.

The calculated transfer function of the antenna can also be used for the modelling of the indoor propagation between different systems. Typically, the transfer functions, that characterise the antennas, are used as input data for propagation tools like ray tracers. In order to illustrate this, the propagation between the DVD player and a Vivaldi antenna is calculated using a simplified analytical formulation of the propagation. The Vivaldi antenna used here is described in detail in [16]. For this paper the original design has been used for an FDTD calculation in order to derive the transfer functions.

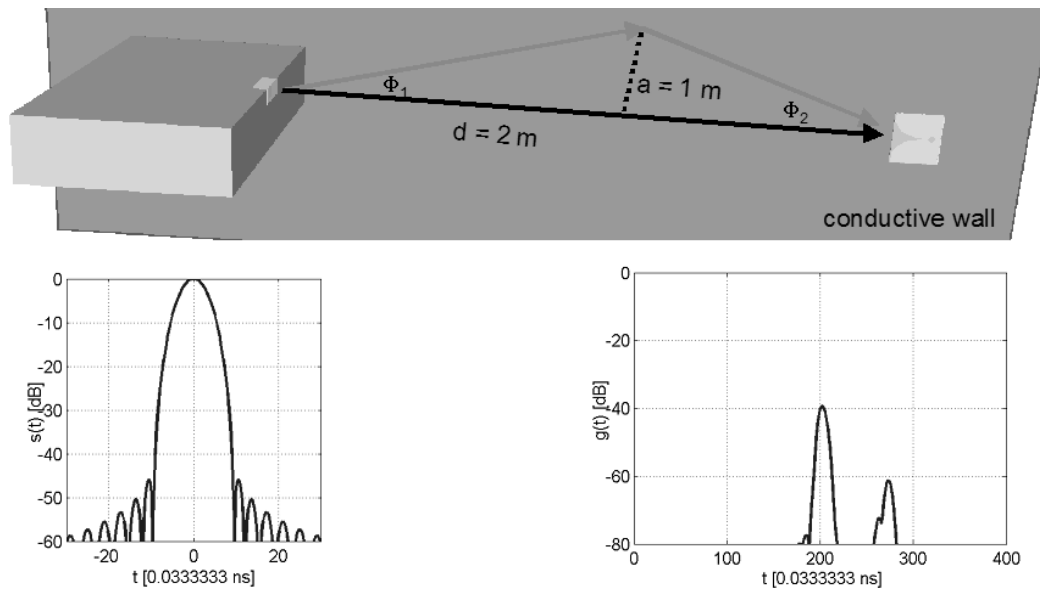


Figure 19: Link between the DVD player and a Vivaldi antenna including one reflection due to a parallel conductive wall. Simplified propagation calculation using the prior assessed transfer functions of the antennas based on the FDTD modeling of the antennas in their specific user situation.

Figure 19 shows the signal used to excite the monocone antenna, and the received signal at the Vivaldi antenna. In addition a reflection from a parallel wall can be observed. The time step in the diagrams is set to 0.033 ns which is the time period a wave propagates over a distance of 1 cm in free space.

3. Conclusion

Today's mobile communication equipment asks for innovative integrated antenna concepts, that are able to handle several frequency bands within one module. Only a global view on the antenna in the environment allows to achieve today's design requirements of integrated antennas in handsets. Future communication systems bring up the necessity to apply this multiband integrated antenna concepts also to modules of other communication systems like PCMCIA cards for PDAs or laptops.

The ultra wideband technologie (UWB) asks for a complete new view on small communication antennas. Not only a good matching of the antenna over the frequency band is required but a stable phase centre to avoid ringing and a good efficiency are necessary to have only a small impact on the transmission function of the radio impulse. Care have to be taken when integrating this antennas in real systems, because the enviroment results in a dramatic change of the performance and new rules have to developed to achieve the best compromise.

4. References

- [1] K. F. Lee, W. Chen (Eds.): *Advances in Microstrip and Printed Antennas*. John Wiley & Sons, New York, 1997.
- [2] J. Ollikainen, O. Kivekäs, A. Toropainen, P. Vainikainen: Internal Dual-Band Patch Antenna for Mobile Phones. AP2000 – Conference on Antennas and Propagation, April 2000, Davos, Switzerland.
- [3] K. F. Tong, K. M. Luk, K. F. Lee, R. Q. Lee: A Broad-Band U-Slot Rectangular Patch Antenna on a Microwave Substrate. In: *IEEE Transactions on Antennas and Propagation*, vol. 48, no. 6, June 2000.
- [4] S. Gonzalez Garcia, L. Baggen, D. Manteuffel, D. Heberling: Study of Coplanar Waveguide-Fed Antennas Using the FDTD Method. *Microwave and Optical Technology Letters*, vol.19, no. 3, S. 173-176, 1998.
- [5] D. Manteuffel, A. Bahr, I. Wolff: Investigation on Integrated Antennas for GSM Mobile Phones. AP2000 – Conference on Antennas and Propagation, April 2000, Davos, Switzerland.
- [6] P. Vainikainen, J. Ollikainen, O. Kivekäs, I. Kelander: Performance Analysis of Small Antennas Mounted on Mobile Handsets. 11th COST 259 Management Committee Meeting, April 2000, Bergen, Norway.
- [7] D. Manteuffel, A. Bahr, Chr. Bornkessel, F. Gustrau, I. Wolff: Fundamental aspects for the design of low-SAR mobile phones. In: *IEE AMS-2002 – Technical Seminar on Antenna Measurement and SAR*, Loughborough, 2002
- [8] T. Taga, “Analysis of planar inverted-F antennas and antenna design for portable radio equipment”, in *Analysis, Design, and Measurement of Small and Low Profile Antennas*, Hirasawa and Haneishi Eds., Artech House, Boston/London, 1992, pp. 161-180.
- [9] H. A. Wheeler, “The radiansphere around a small antenna”, *Proceedings of the IRE*, pp. 1325-1331, August 1959.
- [10] E.H. Newman, P. Bohley, C.H. Walter, „Two Methods for the Measurement of Antenna Efficiency“, *IEEE Trans On Ant. And Propagation*, Vol.AP-23, No. 4, S.457-461, July 1975
- [11] D.M. Pozar, B. Kaufman, „Comparison of Three Methods for the Measurement of Printed Antenna Efficiency“, *IEEE Transactions on Antennas and Propagation*, Vol. 36, No. 1, S. 136-139, January 1988
- [12] M. Geissler, O. Litschke, D. Heberling, P. Waldow, I. Wolff, “An improved method for measuring the radiation efficiency of mobile devices”, *IEEE Antennas & Propagation Symposium*, Columbus, USA, June 2003.
- [13] R.H. Johnston, J. G. McRory, “An Improved Small Antenna Radiation-Efficiency Measurement Method”, *IEEE AP-Magazine*, Vol.40, No.5, October 1998
- [14] Office of Engineering and Technology. Revision of part 15 of the commission’s rules regarding ultra-wideband transmission systems: First report and order. Technical Report FCC 02-48, Federal Communications Commission, Washington, D.C. 20554, April 22, 2002.
- [15] J. Kunisch, J. Pamp: UWB radio channel modeling considerations. In: *Proc. Of ICEAA’03*, Turin, Sep. 2003
- [16] W. Sorgel, C. Waldschmidt, and W. Wiesbeck. Transient responses of a vivaldi antenna and a logarithmic periodic dipole array for ultrawideband communication. 2003 *IEEE Antennas and Propagation Symposium*, June 2003.
- [17] IMST GmbH: User and Reference Manual for the 3D EM Time Domain Simulator Empire, <http://www.empire.de/empire.pdf>, November 2003